ACS Photonics

Article

pubs.acs.org/journal/apchd5

Electronic and Optical Properties of Nanoporous Silicon for Solar-Cell Applications

Guangsha Shi and Emmanouil Kioupakis*

Department of Materials Science and Engineering, University of Michigan, Ann Arbor, Michigan 48109, United States

ABSTRACT: Bulk silicon is a poor light emitter and absorber, but its optical properties are significantly enhanced by nanostructuring. We use first-principles calculations to investigate the electronic and optical properties of nanoporous silicon. We determine and analyze the electronic structure, optical coefficients, and photovoltaic conversion efficiency as a function of pore size and spacing. Our results show that the visible-range absorption coefficient of nanoporous Si is greatly improved compared to the bulk for pore spacings and sizes on the scale of a few nanometers. The photovoltaic efficiency is improved to up to 2.7 times compared to bulk Si, and the theoretical maximum conversion efficiency reaches up to 6.3% for a thin-film nanoporous material thickness of 135 nm. Our results show that nanoporous Si is a promising material for thin-film photovoltaic applications.

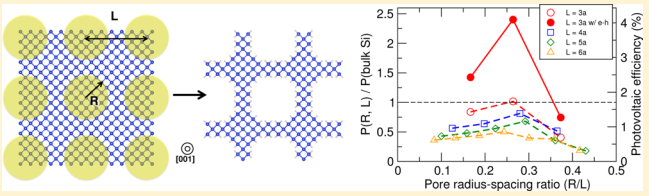

KEYWORDS: *silicon, silicon photonics, nanoporous silicon, optical absorption, exciton, photovoltaic, solar cells, density functional theory*

Silicon is an earth-abundant material of great importance in semiconductor electronics such as integrated circuits and solar cells. However, Si is an indirect-gap semiconductor, and optical transitions across its minimum gap require the assistance of phonons.[1] This results in a low absorption coefficient in the visible range and increases the material thickness and cost for photovoltaic applications. The indirect band gap of bulk Si also makes it an inefficient light emitter and precludes its applications for active optoelectronic components. Increasing the light absorption and emission in Si could extend the already established Si manufacturing technology into optoelectronics and has been an area of intense research activity.

Nanostructuring is a promising approach to engineer the optical properties of Si and increase the efficiency of thin-film Si solar cells. Pattering the surface of Si with nanopores of 220 nm diameter has been demonstrated to reduce the surface reflection to less than 5% and increase optical absorption in the visible range.[2] Moreover, Si nanowires with a diameter of 390 nm increase the optical path length in thin-film solar cells by up to a factor of 73 and deliver efficiencies above 5%.[3] Similar Si nanowire array geometries have been found to suppress reflectivity and improve absorption in the visible range.[4,5] The structural features of the above-mentioned Si nanostructures are on the order of 100 nm, which is comparable to the wavelength of visible photons and therefore has a strong effect on wave propagation and reflection in solar cells made of these nanostructures. However, nanostructures of this scale do not exhibit strong quantum confinement, and the fundamental electronic properties of Si (e.g., band gap, exciton binding energy, optical matrix elements) are not affected significantly compared to the bulk. Nanostructuring with pores of 60 nm diameter has been demonstrated to enable optical gain and stimulated emission in nanoporous crystalline Si, but this is attributed to recombination at A-center defects.[6]

Si nanostructures with features on the scale of a few nanometers are strongly affected by quantum confinement, and their optical absorption and emission properties can be significantly enhanced compared to the bulk. Besides increasing the band gap, quantum confinement breaks the momentum-conservation requirement along the confinement direction and increases the probability of optical transitions across the indirect band gap. Nanostructuring can thus enable the emission of visible light from Si. Visible photoluminescence at room temperature has been reported for Si quantum wire arrays with features on the 5 nm scale.[7] Luminescence has also been reported in 1 nm wide Si nanoparticles that can be tailored through modification of the surface chemistry.[8] Moreover, highly efficient and color-tunable visible LEDs have been fabricated with Si nanocrystals with a size between 1 and 2 nm.[9]

Previous theoretical work has examined the electronic and optical properties of a range of nanometer-sized Si nanostructures. Van de Walle and Northrup investigated the electronic properties of Si-based layered structures using first-principles methods.[10] They found that a two-layer Si structure has a direct band gap and a strong direct transition between the band-edge states. Hybertsen studied the phonon-assisted and zero-phonon transitions in Si nanostructures and found that phonon-assisted processes dominate optical transitions for nanofeature sizes above 1.5 to 2 nm.[11] A genetic algorithm was employed by d'Avezac et al. to search for all possible Si/Ge superlattices and

Received: August 10, 2014
Published: December 2, 2014

DOI: 10.1021/ph5002999
ACS Photonics 2015, 2, 208−215

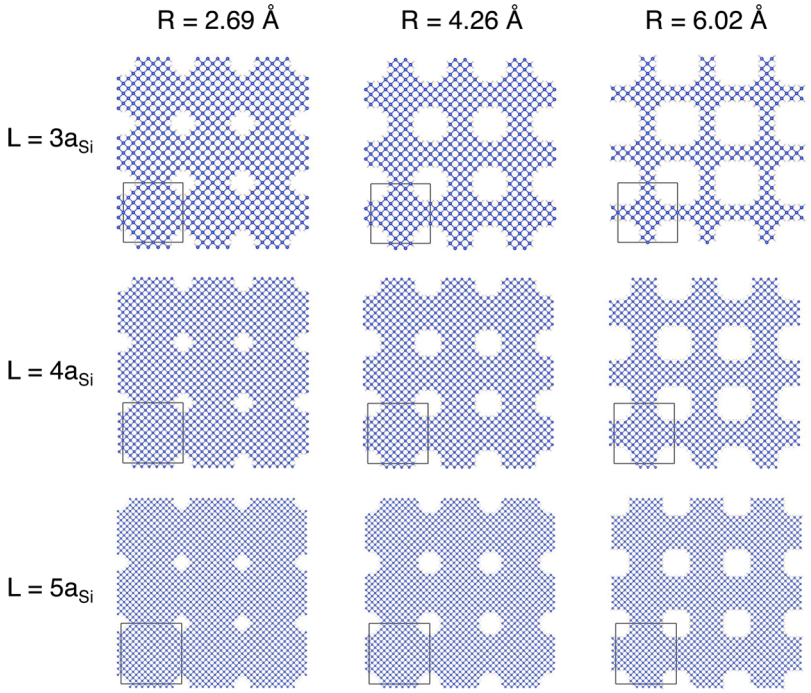

Figure 1. Some of the nanoporous Si structures with various pore radius R and pore spacing L examined in this work. Quantum confinement by the nanoscale pores increases the probability of optical transitions across the band gap of Si and enhances the absorption coefficient in the visible range.

found one specific configuration with a direct band gap and a strong dipole-allowed transition.[12] Direct band gaps were also observed by Peelaers et al. for Si/Ge core−shell nanowires with a diameter of 1.2 to 1.6 nm[13] and by Yang et al. for Si nanowires with a diameter of 1.2 nm.[14] Moreover, a large exciton binding energy (0.8−1.1 eV) was reported by Yang et al.[14] and by Bruno et al.[15] for Si nanowires with a diameter less than 2 nm. The strong excitonic effects in these nanostructures are attributed to the enhanced electron−hole interaction due to the quantum confinement. This body of theoretical work provides strong evidence that Si nanostructures with characteristic features on the order of a few nanometers are very promising for optoelectronic applications.

Nanoporous Si presents the advantage that the pores introduce quantum confinement and carrier scattering only in two of the three spatial dimensions. Thus, nanopores cause the scattering of electrons by the pore sidewalls and enable the absorption of light with polarization perpendicular to the pore direction. However, at the same time nanopores do not strongly affect carrier scattering or carrier mobility along the pore direction and, thus, allow for high carrier-extraction efficiency. As a result, thin-film nanoporous Si may overcome the stability and efficiency limitations of disordered hydrogenated amorphous Si, which suffers from the detrimental Staebler−Wronski effect.[16]

In this work we present and analyze the electronic and optical characteristics of nanoporous Si with nanoscale patterns on the order of a few nanometers. Quantum confinement by the nanopores increases the band gap and enhances carrier scattering, thus improving the optical absorption that is desired in solar-cell applications. We show that nanoporous Si can exhibit simultaneously improved absorption, reduced reflectivity, and increased photovoltaic conversion efficiency compared to bulk Si. Our results indicate that the photovoltaic efficiency of nanoporous Si can be improved by up to 2.7 times compared to the bulk for a film thickness of 135 nm and that the maximum absolute conversion efficiency in nanoporous Si can reach up to 6.3%. Therefore, nanoporous Si thin films can have a higher photovoltaic conversion efficiency than thin-film bulk Si and a substantially increased efficiency to material cost ratio than commercial bulk Si solar cells and could be applied to develop low-cost and flexible Si solar cells with an appreciable efficiency.

RESULTS AND DISCUSSION

Structure. Figure 1 shows some of the nanoporous Si structures examined in this work. The structural models were constructed by perforating bulk Si with nanoscale pores of radius R and spacing L along the [001] direction. Although hexagonal pore patterns are encountered experimentally, we considered a square-lattice distribution of pores because the hexagonal lattice is incommensurate with the symmetry of the (001) surface of Si and results in too large simulation cells. We expect that a hexagonal pore arrangement yields similar results to the investigated square pore arrangement for the electronic and optical properties and the photovoltaic efficiency enhancement as a function of pore size and spacing. We investigated a total of 20 nanoporous Si structures with pore spacing up to 6 times the lattice constant of the conventional unit cell of bulk Si (a_{Si} = 5.43 Å) and pore radius ranging from 2.7 to 13.5 Å. The Si dangling bonds on the nanopore surfaces were passivated with H atoms to eliminate midgap defect states that contribute to nonradiative recombination. Chemical passivation by oxygen,[17] methyl[18] (CH_3), and halogen[19] is used in practice to eliminate surface dangling bonds in porous Si and Si nanowires for higher ambient stability. The nanoporous Si systems we studied are all intrinsic. The additional screening and absorption by free carriers are weak at typical solar irradiation conditions and are not expected to affect the calculated results. We studied nanostructures containing up to 300 atoms in the periodic cell, and GW calculations for the

DOI: 10.1021/ph5002999
ACS Photonics 2015, 2, 208−215

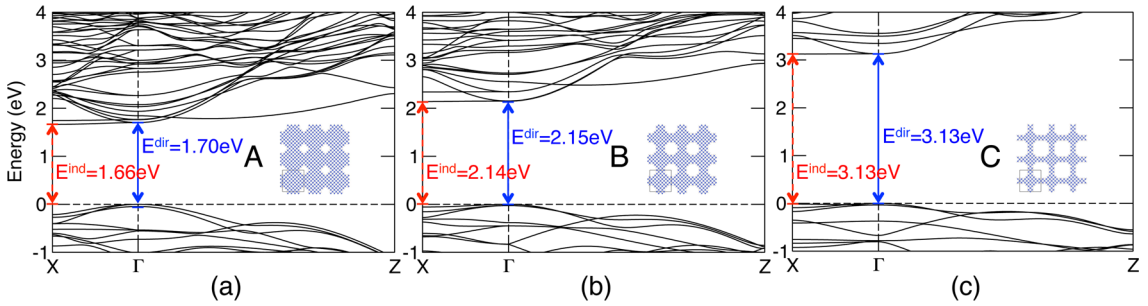

Figure 2. Band structures of three of the investigated nanoporous Si structures (*A*, *B*, and *C* shown in the insets).

largest simulation cells required up to 10 000 CPU hours. All structures were relaxed to minimize the stress and the forces on the atoms.

Band Structure. Figure 2 shows the band structures of three nanoporous Si structures [*A* ($L = 3a_{Si}$, $R = 2.69$ Å), *B* ($L = 3a_{Si}$, $R = 4.26$ Å), and *C* ($L = 3a_{Si}$, $R = 6.02$ Å)] along the in-plane (Γ−X) and out-of-plane (Γ−Z) directions. These three structures have the same pore spacing but different pore radii. As the pore size increases, the band gap widens from 1.66 eV to 3.13 eV due to increasing quantum confinement. The band gap of structures *A* and *B* is indirect with the valence-band maximum located at the Γ point and the conduction-band minimum located at the X point. The difference between the minimum direct and the indirect gap, however, decreases to below 1 meV for structure *C*, and thus direct transitions also contribute to optical absorption near the onset for this structure. Since the conduction-band minimum of bulk Si is located at a point between Γ and X, the shift of the conduction-band minimum in nanoporous Si is attributed to band structure distortion by the introduction of nanopores. The lowest conduction band gets flatter along the quantum-confined direction as the pore radius increases and becomes almost horizontal for structure *C*.

The band gap of nanoporous Si as a function of pore radius and spacing is shown in Figure 3. Most structures are found to

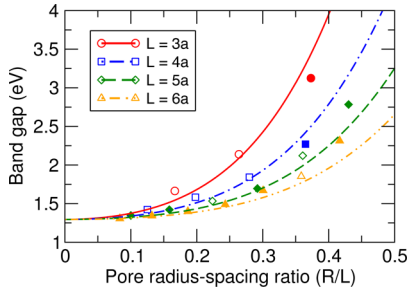

Figure 3. Band-gap values of nanoporous Si as a function of pore radius and spacing. The lines are fits to the calculated data. The structures with direct band gaps are marked with solid symbols.

have quasi-direct band gaps and are marked with solid symbols in Figure 3. The band gaps tend to be quasi-direct for large pore spacing, which is the case for most examined structures with $L = 5a_{Si}$ or $L = 6a_{Si}$. This is explained by the multiple folding of the Brillouin zone along the quantum-confined direction. The gap is also more likely to be quasi-direct for structures with large pore size, a trend already analyzed for structures *A*, *B*, and *C*. The band gap values were fitted as a function of pore radius *R* and spacing *L* according to

$$E_{gap}(R, L) = E_{gap}^{bulk} + \frac{1}{L^2} f\left(\frac{R}{L}\right) \quad (1)$$

where the calculated band gap of bulk Si, E_{gap}^{bulk}, is 1.295 eV (which is within the typical 0.1 eV accuracy of the computational method compared to the experimental value of 1.17 eV at 0 K[20]), and $f(x)$ is a shape-dependent term representing different levels of confinement for different values of the R/L ratio, which was found to be $f(x) = (1923x^2 + 14976x^4)$ eV Å^2.

Optical Matrix Elements. Although most nanoporous structures with large pore spacings have a quasi-direct band gap, the transition probability across these gaps is small compared to typical direct-gap transitions. Figure 4 shows the average optical

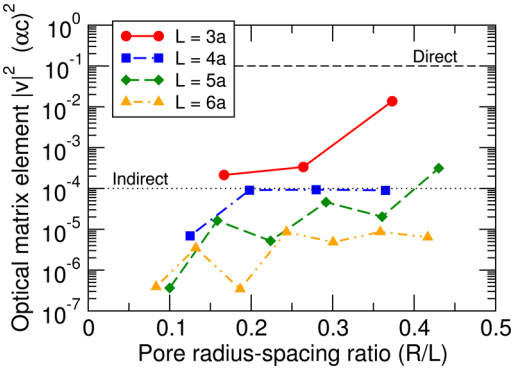

Figure 4. Average optical (velocity) matrix elements squared of interband transitions between the states within 100 meV from the band edges of the investigated nanoporous Si structures at the Γ point for light polarized perpendicular to the pore direction. The optical matrix elements are given in units of $(\alpha c)^2$, where α is the fine-structure constant and c is the speed of light. The horizontal dashed line indicates the typical value of direct optical transition matrix elements across the direct gap of bulk Si at the Γ point, while the dotted line denotes the characteristic value of indirect (phonon-assisted) optical matrix elements across the indirect gap of bulk Si.

(velocity) matrix elements of interband transitions between states within 100 meV from the band edges at the Γ point for light polarized perpendicular to the pore direction. The optical matrix elements for all examined structures are smaller than the typical value for the direct allowed transition in bulk Si at the Γ point, and for most structures they are also smaller than the typical indirect (phonon-assisted) optical transition matrix elements of bulk Si (Figure 4). Therefore, the reported direct gaps of Figure 3 are quasi-direct since they are associated with small transition probabilities. Only the matrix elements for the smallest pore spacing ($L = 3a_{Si}$) are larger than the characteristic value of phonon-assisted transitions. This is in

DOI: 10.1021/ph5002999
ACS Photonics 2015, 2, 208−215

agreement with the earlier work of Hybertsen,[11] who found that phonons are the dominant carrier-scattering mechanism that mediates optical transitions in Si for nanoscale features larger than 1.5 to 2 nm. The transition probability across the band gap is largest when quantum confinement is strongest (large pore radius and small pore spacing) and decreases with decreasing degree of quantum confinement. In the limit of small pore size and large pore separation the matrix elements approach zero, since this is the limit of the transition across the indirect gap of bulk Si, which is forbidden without the assistance of phonons.

Dielectric Constant. The dielectric constants of all studied nanoporous Si structures are summarized in Figure 5. Screening

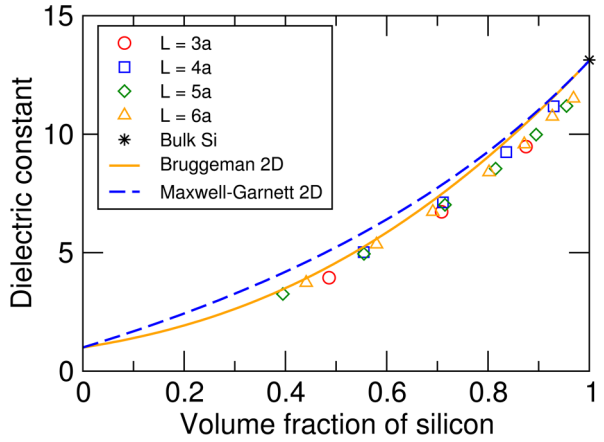

Figure 5. Dielectric constant of nanoporous Si as a function of Si volume fraction for various pore geometries. The data are in very good agreement with both the Bruggeman formula (solid) and the Maxwell−Garnett formula (dashed).

is enhanced for increasing Si volume fraction. The first-principles results are in good agreement with both the 2D Bruggeman nonsymmetric model,[21]

$$f_{Si} = \frac{1 - \varepsilon_{eff}}{1 - \varepsilon_{Si}} \left(\frac{\varepsilon_{Si}}{\varepsilon_{eff}} \right)^{1/2} \tag{2}$$

and the 2D Maxwell−Garnett model,[22]

$$\frac{\varepsilon_{eff} - \varepsilon_{Si}}{\varepsilon_{eff} + \varepsilon_{Si}} = (1 - f_{Si}) \frac{1 - \varepsilon_{Si}}{1 + \varepsilon_{Si}} \tag{3}$$

where ϵ_{Si} and ϵ_{eff} are the dielectric constants of bulk and nanoporous Si, respectively. The 2D Maxwell−Garnett model considers vacuum cylinder inclusions in a matrix of bulk Si, while the 2D Bruggeman model treats both Si and vacuum as cylindrical inclusions in a theoretical effective medium. The Bruggeman model is thus an extension of the Maxwell−Garnett model.[23] Our first-principles results show that both models are similarly valid in describing the dielectric constant of porous Si at the nanoscale.

Optical Properties. To understand the effect of quantum confinement on the optical properties of nanoporous Si, we examine the real (ϵ_1) and imaginary (ϵ_2) parts of the dielectric function for structures *A* and *B* and compare it to the dielectric function of bulk Si (Figure 6). A Gaussian function with a width of 0.15 eV was used to account for the broadening of the optical spectra. For the purposes of this analysis, only direct optical transitions (no phonon-assisted absorption) across the

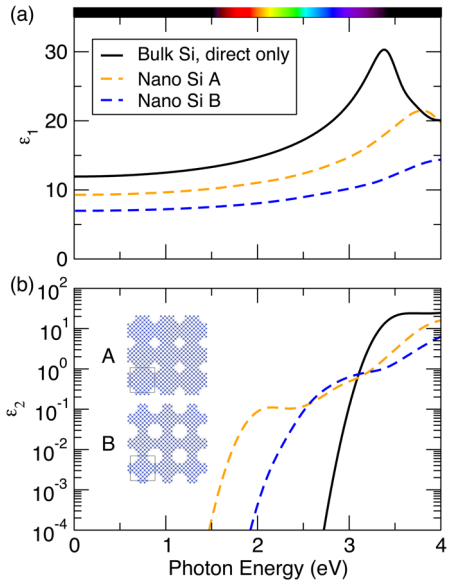

Figure 6. Dielectric functions of structures *A* and *B* compared to bulk Si. (a) Real part (ϵ_1) and (b) imaginary part (ϵ_2). Electron scattering by the nanoscale pores enables optical transitions across the gap in structures *A* and *B*. Only direct optical transitions are considered for bulk Si (no phonon-assisted transitions), and only direct and quasi-direct transitions are included for the nanostructures to highlight the additional absorption due to the quasi-direct transitions in nanoporous Si.

direct gap of bulk Si have been included in Figure 6. The two nanoporous Si structures have the same pore spacing but different pore radii. Structure *A* has a larger ϵ_1 than structure *B* and is closer to bulk Si (Figure 6a). This is because structure *A* exhibits stronger screening effects than structure *B* due to its higher Si volume fraction. The imaginary part curves (Figure 6b) show that the direct absorption edges for both examined nanoporous Si structures occur at lower energies (1.70 eV for structure *A* and 2.15 eV for structure *B*, Figure 2) than the first direct optical transition of bulk Si (3.4 eV[24]), which indicates that scattering of electrons by the nanopores enables quasi-direct optical transitions across the band gap. The refractive index *n* and the extinction coefficient κ are determined from ϵ_1 and ϵ_2 using

$$n(E) = \frac{1}{\sqrt{2}} \sqrt{\varepsilon_1(E) + \sqrt{\varepsilon_1^2(E) + \varepsilon_2^2(E)}} \tag{4}$$

and

$$\kappa(E) = \frac{1}{\sqrt{2}} \sqrt{-\varepsilon_1(E) + \sqrt{\varepsilon_1^2(E) + \varepsilon_2^2(E)}} \tag{5}$$

where *E* is the photon energy. The reflectivity and absorption coefficient were calculated from *n* and κ by

$$R(E) = \frac{(n-1)^2 + \kappa^2}{(n+1)^2 + \kappa^2} \tag{6}$$

and

$$\alpha(E) = \frac{4\pi\kappa}{hc/E} \tag{7}$$

and are shown as a function of photon energy for nanoporous Si structures *A* and *B* in Figure 7. Structure *B* shows lower reflectivity (Figure 7a) and larger optical gap (Figure 7b) than

DOI: 10.1021/ph5002999
ACS Photonics 2015, 2, 208−215

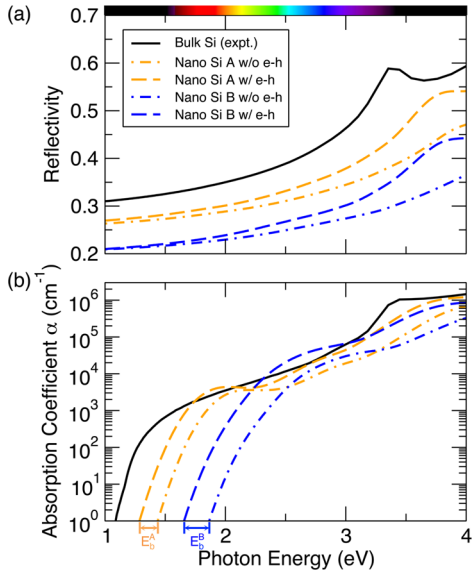

Figure 7. (a) Reflectivity and (b) absorption coefficient of nanoporous Si structures *A* and *B*. Dashed lines include excitonic effects due to electron−hole (e−h) interaction, while dash-dot lines do not include excitonic effects. The calculated results are also compared to the experimental data for bulk Si.

structure *A* and bulk Si[25] because of its lower Si volume fraction and stronger quantum confinement. Strong confinement in structure *B* also leads to stronger pore-electron scattering, which gives higher electron transition probability and absorption coefficient than both structure *A* and bulk Si in the 2.3−3.2 eV energy range (Figure 7b). We note that we did not include phonon-assisted optical transitions for nanoporous Si, which would increase the absorption even further.

Excitons. We studied excitonic effects in nanoporous Si arising from the electron−hole interaction. Excitonic effects have been shown by first-principles calculations to modify the optical coefficients of bulk Si due to the coherent coupling of different electron−hole configurations.[26,27] In quantum-confined structures such as nanowires[14,15,28] excitonic effects additionally increase the exciton binding energy and shift the onset of optical absorption to lower energies. Structure *B* has a larger exciton binding energy (0.23 eV) than structure *A* (0.13 eV) since the increased quantum confinement enhances the strength of the electron−hole interaction (Figure 7b). Although the exciton binding energy of the examined nanoporous structures *A* and *B* is increased by an order of magnitude compared to bulk Si (15 meV),[27] it is 1 order of magnitude smaller than that of Si nanowires with comparable confinement radius (0.8−1.1 eV) determined from theoretical predictions.[14,15] This is attributed to the weaker quantum confinement in nanoporous Si than nanowires since the Si regions are connected in the nanoporous geometry and have a larger confinement volume for the same linear confinement dimension (Figure 1).

Photovoltaic Conversion Efficiency. Our predictive results can be applied to answer whether nanopores can improve the photovoltaic conversion efficiency of thin-film Si solar cells and to identify promising nanoporous Si structures for photovoltaic applications. The calculated reflectivity and absorption coefficient are two important factors that affect the photovoltaic conversion efficiency, defined as the fraction of solar energy converted to electrical power per unit area of material. The electrical power density is calculated by integrating the converted spectral irradiance over the solar-spectrum wavelengths:

$$P = \int_0^{\lambda_{max}} W(\lambda)[1 - R(\lambda)]A(\lambda)\, C(\lambda)\, d\lambda \tag{8}$$

where λ is the photon wavelength, λ_{max} is the longest wavelength that can be absorbed by the nanostructure and is determined by the direct band gap of the nanoporous Si structure,

$$\lambda_{max} = \frac{hc}{E_g^{dir}} \tag{9}$$

and $W(\lambda)$ is the solar spectral irradiance at Air Mass 1.5.[29] The term $R(\lambda)$ is the reflectivity of the front surface of the material, and the absorbance $A(\lambda)$ is given by

$$A(\lambda) = 1 - e^{-\alpha(\lambda)d} \tag{10}$$

where d is the thickness of the material. The term $C(\lambda)$ is a conversion factor to account for the fraction of the photon energy converted to electronic energy (i.e., to the excitation energy of one electron−hole pair across the minimum band gap),

$$C(\lambda) = \lambda\frac{E_g}{hc} \tag{11}$$

where E_g is the minimum (direct or indirect) band gap of the material.

Several competing factors affect the photovoltaic conversion efficiency of thin-film nanoporous Si compared to bulk. Decreasing the volume fraction of Si in the nanostructures reduces the reflectivity on the front surface and increases the fraction of solar photons that enter the material. Moreover, quantum confinement by the nanopores enables pore-electron scattering and enhances the absorption of solar photons. In addition, the increased band gap of nanoporous Si results in a higher fraction of converted photon energy (eq 11) and increased converted power density. On the other hand, larger band-gap values in the nanostructures blue-shift the absorption edge and reduce the absorption of long-wavelength photons. To explore how these competing effects affect the photovoltaic conversion efficiency of thin-film Si, we calculated the electrical power of all 20 structures for a material thickness of 100 nm using eq 8. The relative converted electrical power for the nanoporous structures compared to bulk Si is shown in Figure 8 as a function of pore radius and spacing. The data show that the introduction of nanopores can indeed improve the efficiency over the bulk. Among all the nanostructures studied, structure *B* ($L = 3a_{Si}$ and $R = 4.26$ Å) exhibits the highest converted electrical power density (eq 8), which is about 2.5 times that of bulk Si for the considered thin-film thickness of 100 nm. If, in addition, we assume the effect of an antireflective coating to suppress the surface reflectivity of both bulk Si and structure *B*, the efficiency ratio decreases from 2.5 to 1.9, but the absolute efficiency of structure *B* increases from 4.1% to 5.9%. The structures with the smallest pore spacing show the highest conversion efficiencies for this material thickness. For fixed pore spacing the converted power first increases with increasing pore radius, due to the enhanced pore-electron scattering and increased converted electrical energy, followed by a decrease due to the blue-shift of the absorption threshold that cancels out the other advantages of nanostructuring. The

DOI: 10.1021/ph5002999
ACS Photonics 2015, 2, 208−215

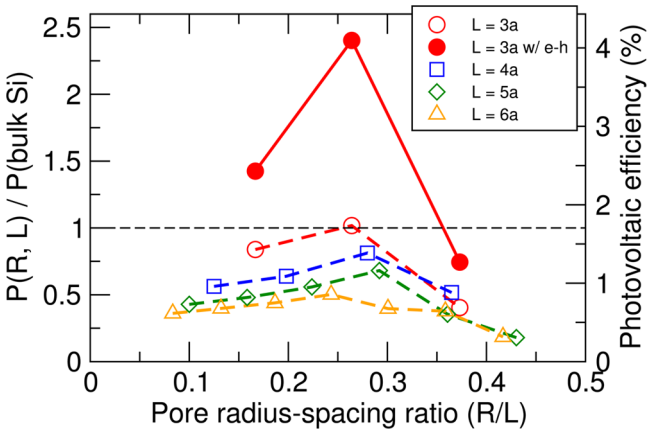

Figure 8. Relative converted electrical power produced in nanoporous Si compared to the bulk as a function of pore radius and spacing. A thin-film material thickness of 100 nm is assumed. The data show that nanoporous Si structures with pore spacing on the order of 3 times the lattice constant of bulk Si (16.3 Å) can exceed the photovoltaic efficiency of an equivalent bulk Si structure. Excitonic effects have only been considered for the smallest nanopore structures due to the computational cost of the calculations. Phonon-assisted optical processes that further increase the absorption coefficient have not been included in the absorption spectra of the nanostructures.

optimized photovoltaic conversion efficiency is achieved for small pore spacing and a radius-to-spacing ratio around 0.25 to 0.30. We note that excitonic effects have a significant effect on the efficiency of nanoporous Si and increase the converted power by as much as a factor of 2.5. We also note that phonon-assisted absorption, which is the only absorption mechanism of visible light in bulk Si, has not been considered for the nanoporous structures. If electron−phonon scattering is also considered for the nanostructures (in addition to electron-pore scattering), then the conversion efficiency is expected to increase further.

Our data can identify which photon wavelengths contribute the most to the produced electrical power for each Si structure. As an example, Figure 9 presents a comparison of the converted power density of nanoporous structures *A* and *B* with bulk Si analyzed in terms of absorbed photon wavelength for a material thickness of 100 nm. The location of the peak of the converted spectral irradiance for each structure is determined from the

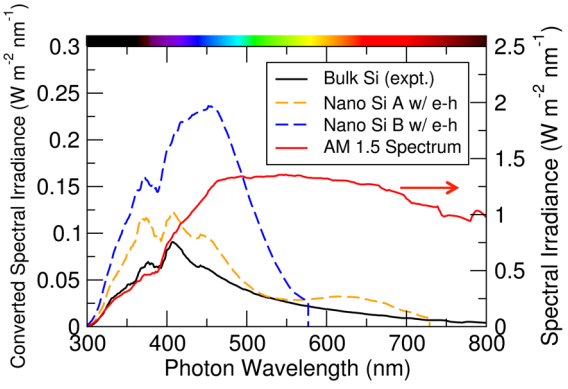

Figure 9. Converted spectral irradiance per unit area for nanoporous Si structures *A* and *B* and compared to bulk Si. The integrated area under each curve yields the converted electrical power per unit area for each structure. A material thickness of 100 nm is assumed.

combined wavelength dependence of the solar irradiance, the reflectivity, and the absorption coefficient. The spectral peak for nanoporous Si structure *B* occurs at a longer wavelength than structure *A* and bulk Si because the absorption spectrum for structure *B* exhibits a peak at 2.7 eV (460 nm) (Figure 7b), which corresponds to large values of the solar irradiance.

In thin-film nanoporous Si structures the effect from Fabry−Perot resonance may not be neglected, and reflections between the front and back surface should also be considered. In this case, the photovoltaic conversion efficiency is defined as

$$P = \int_0^{\lambda_{max}} W(\lambda)[1 - R(\lambda) - T(\lambda)]C(\lambda)\,d\lambda \tag{12}$$

where $R(\lambda)$ and $T(\lambda)$ are the reflectivity and transmissivity,

$$R(\lambda) = \left| r_1 - \frac{t_1^2 r_2 e^{-i\delta}}{1 - r_1 r_2 e^{-i\delta}} \right|^2 \tag{13}$$

and

$$T(\lambda) = \left| \frac{-t_1 t_2 e^{-i\delta}}{1 - r_1 r_2 e^{-i\delta}} \right|^2 \tag{14}$$

The quantities $r_{1,2}$ and $t_{1,2}$ are the amplitude factors of the reflected and transmitted field at the front and back surface. The phase factor δ is defined as

$$\delta = \frac{2\pi\tilde{n}d}{\lambda} \tag{15}$$

where $\tilde{n}$ is the complex refractive index. Thin-film effects introduce oscillations in the efficiency curves (Figure 10) due

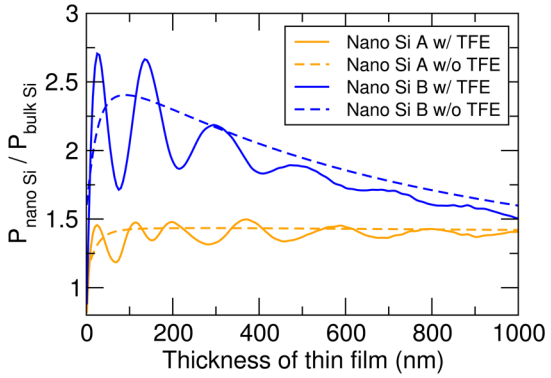

Figure 10. Converted electrical power produced in nanoporous Si structures *A* and *B* as a function of material thickness relative to bulk Si including thin-film effects. The conversion efficiency for structure *B* has pronounced maxima for a thin-film thickness of 25 and 135 nm.

to the periodicity of the reflectivity and transmissivity with material thickness. The advantages of nanoporous Si compared to the bulk material for energy conversion are more pronounced in the 100 nm thickness regime. The nanoporous Si structure *B* shows the largest enhancement of conversion efficiency over bulk Si by a factor of 2.7 at the two peaks that correspond to a thickness of 25 and 135 nm. Assuming the solar irradiance based on the direct standard AM 1.5 spectrum, nanoporous Si structure *B* has a photovoltaic conversion efficiency of 1.5% for a material thickness of 25 nm and 6.3% at a thickness of 135 nm. We note that a full investigation of solar-cell efficiency requires knowledge of the impact of defects on

DOI: 10.1021/ph5002999
ACS Photonics 2015, 2, 208−215

the device performance, as well as a number of other efficiency loss mechanisms (e.g., nonradiative recombination, energy loss at interfaces, etc.). However, defect simulations for these nanostructures are challenging, while the nature and concentration of defects depend on the growth conditions of the sample. In the present study we focus on the fundamental energy-conversion properties; therefore the efficiency we estimate constitutes an upper limit value. Nevertheless, our predictive calculations show that nanoporous Si with pore size and spacing on the scale of a few nanometers can indeed exhibit improved photovoltaic performance over bulk Si and can yield a theoretical maximum conversion efficiency of a few percent in thin-film solar-cell applications.

CONCLUSIONS

In conclusion, we used first-principles methods to calculate the electronic and optical properties of nanoporous Si with pore spacing and radius on the order of a few nanometers. We found that the inclusion of nanoscale pores increases the electronic band gaps due to quantum confinement and results in quasi-direct gaps for most examined structures. The visible-range absorption coefficient is greatly improved in nanoporous Si with small pore spacings and appropriately chosen pore sizes. Although quantum confinement reduces the wavelength range for the absorption of solar photons, the enhanced absorption coefficient as well as the reduced reflectivity and increased band gap improve the photovoltaic efficiency compared to bulk Si by a factor of 2.7 and yields a theoretical maximum conversion efficiency of 6.3% for thin-film (135 nm thick) solar cells.

Therefore, the enhanced electronic and optical properties of nanoporous Si make it a promising material for thin-film photovoltaic applications.

METHODS

We studied the electronic and optical properties of nanoporous Si using first-principles calculations based on density functional theory (DFT) and many-body perturbation theory. We performed DFT calculations to obtain the ground-state charge density and electronic wave functions using the local-density approximation[30,31] for the exchange−correlation potential. We used the plane-wave pseudopotential method[32] with a plane-wave cutoff of 16 Ry and norm-conserving pseudopotentials[33] as implemented in the Quantum-ESPRESSO code.[34] We calculated the quasi-particle band energies of nanoporous Si using the one-shot GW method[35] and the BerkeleyGW code.[36] The static dielectric function was calculated with a 7 Ry plane-wave cutoff and extended to finite frequency using the generalized plasmon-pole model of Hybertsen and Louie.[35] The Coulomb-hole self-energy term was calculated using a sum over three times as many unoccupied bands as occupied bands using the static-remainder approach.[37] The dielectric function was calculated using all occupied bands and unoccupied bands up to 7.5 eV above the valence-band maximum. The quasi-particle energies of the nanoporous Si structures with $L = 3a_{Si}$ were calculated with a 2 × 2 × 4 Monkhorst−Pack[38] mesh, while the other structures with larger unit cells were studied with a 1 × 1 × 4 Monkhorst−Pack mesh. We also used the Bethe−Salpeter equation formalism[27] to study two-particle excitations and calculate the optical absorption and reflectivity spectra including excitonic effects. Excitonic effects on the optical absorption spectra have been considered only for the three examined structures *A*, *B*, and *C* with the smallest pore spacing ($L = 3a_{Si}$) due to the high computational expense of Bethe−Salpeter calculations for larger structures.

AUTHOR INFORMATION

Corresponding Author

*E-mail: kioup@umich.edu.

Notes

The authors declare no competing financial interest.

ACKNOWLEDGMENTS

We thank Dylan Bayerl and Jack Deslippe for helpful discussions. This work was supported as part of CSTEC, an Energy Frontier Research Center funded by the U.S. Department of Energy, Office of Science, Basic Energy Sciences, under Award DE-SC0000957. Computational resources were provided by the National Energy Research Scientific Computing Center, which is supported by the Office of Science of the U.S. Department of Energy under Contract No. DE-AC02-05CH11231.

REFERENCES

(1) Noffsinger, J.; Kioupakis, E.; Van de Walle, C. G.; Louie, S. G.; Cohen, M. L. Phonon-Assisted Optical Absorption in Silicon from First Principles. *Phys. Rev. Lett.* **2012**, *108*, 167402.

(2) Liu, Y.; Sun, S.; Xu, J.; Zhao, L.; Sun, H.; Li, J.; Mu, W. W.; Xu, L.; Chen, K. J. Broadband Antireflection and Absorption Enhancement by Forming Nano-Patterned Si Structures for Solar Cells. *Opt. Express* **2011**, *19*, A1051−A1056.

(3) Garnett, E.; Yang, P. Light Trapping in Silicon Nanowire Solar Cells. *Nano Lett.* **2010**, *10*, 1082−1087 PMID: 20108969.

(4) Zhu, J.; Yu, Z.; Burkhard, G. F.; Hsu, C.-M.; Connor, S. T.; Xu, Y.; Wang, Q.; McGehee, M.; Fan, S.; Cui, Y. Optical Absorption Enhancement in Amorphous Silicon Nanowire and Nanocone Arrays. *Nano Lett.* **2009**, *9*, 279−282.

(5) Tsakalakos, L.; Balch, J.; Fronheiser, J.; Korevaar, B. A.; Sulima, O.; Rand, J. Silicon Nanowire Solar Cells. *Appl. Phys. Lett.* **2007**, *91*, 233117.

(6) Cloutier, S. G.; Kossyrev, P. A.; Xu, J. Optical Gain and Stimulated Emission in Periodic Nanopatterned Crystalline Silicon. *Nat. Mater.* **2005**, *4*, 887−891.

(7) Canham, L. T. Silicon Quantum Wire Array Fabrication by Electrochemical and Chemical Dissolution of Wafers. *Appl. Phys. Lett.* **1990**, *57*, 1046−1048.

(8) Eckhoff, D. A.; Sutin, J. D. B.; Clegg, R. M.; Gratton, E.; Rogozhina, E. V.; Braun, P. V. Optical Characterization of Ultrasmall Si Nanoparticles Prepared through Electrochemical Dispersion of Bulk Si. *J. Phys. Chem. B* **2005**, *109*, 19786−19797.

(9) Maier-Flaig, F.; Rinck, J.; Stephan, M.; Bocksrocker, T.; Bruns, M.; Kübel, C.; Powell, A. K.; Ozin, G. A.; Lemmer, U. Multicolor Silicon Light-Emitting Diodes (SiLEDs). *Nano Lett.* **2013**, *13*, 475−480.

(10) Van de Walle, C. G.; Northrup, J. E. *Porous Silicon*; Chapter 16, pp 329−344.

(11) Hybertsen, M. S. Absorption and Emission of Light in Nanoscale Silicon Structures. *Phys. Rev. Lett.* **1994**, *72*, 1514−1517.

(12) d'Avezac, M.; Luo, J.-W.; Chanier, T.; Zunger, A. Genetic-Algorithm Discovery of a Direct-Gap and Optically Allowed Superstructure from Indirect-Gap Si and Ge Semiconductors. *Phys. Rev. Lett.* **2012**, *108*, 027401.

(13) Peelaers, H.; Partoens, B.; Peeters, F. M. Electronic and Dynamical Properties of Si/Ge Core-Shell Nanowires. *Phys. Rev. B* **2010**, *82*, 113411.

(14) Yang, L.; Spataru, C. D.; Louie, S. G.; Chou, M. Y. Enhanced Electron-Hole Interaction and Optical Absorption in a Silicon Nanowire. *Phys. Rev. B* **2007**, *75*, 201304.

DOI: 10.1021/ph5002999
ACS Photonics 2015, 2, 208−215

(15) Bruno, M.; Palummo, M.; Marini, A.; Del Sole, R.; Ossicini, S. From Si Nanowires to Porous Silicon: The Role of Excitonic Effects. *Phys. Rev. Lett.* **2007**, *98*, 036807.
(16) Staebler, D. L.; Wronski, C. R. Optically Induced Conductivity Changes in Discharge-Produced Hydrogenated Amorphous Silicon. *J. Appl. Phys.* **1980**, *51*, 3262−3268.
(17) Wu, X. L.; Xiong, S. J.; Fan, D. L.; Gu, Y.; Bao, X. M.; Siu, G. G.; Stokes, M. J. Stabilized Electronic State and Its Luminescence at the Surface of Oxygen-Passivated Porous Silicon. *Phys. Rev. B* **2000**, *62*, R7759−R7762.
(18) Haick, H.; Hurley, P. T.; Hochbaum, A. I.; Yang, P.; Lewis, N. S. Electrical Characteristics and Chemical Stability of Non-Oxidized, Methyl-Terminated Silicon Nanowires. *J. Am. Chem. Soc.* **2006**, *128*, 8990−8991 PMID: 16834345.
(19) Buriak, J. M. Organometallic Chemistry on Silicon and Germanium Surfaces. *Chem. Rev.* **2002**, *102*, 1271−1308 PMID: 11996538..
(20) Bludau, W.; Onton, A.; Heinke, W. Temperature Dependence of the Band Gap of Silicon. *J. Appl. Phys.* **1974**, *45*, 1846.
(21) Bruggeman, D. A. G. Berechnung Verschiedener Physikalischer Konstanten von Heterogenen Substanzen. I. Dielektrizitätskonstanten und Leitfähigkeiten der Mischkörper aus Isotropen Substanzen. *Ann. Phys. (Weinheim, Ger.)* **1935**, *416*, 636−664.
(22) Van Beek, L. Dielectric Behaviour of Heterogeneous Systems. *Prog. Dielectr.* **1967**, *7*, 69−114.
(23) Torres-Costa, V.; Martin-Palma, R. In *Porous Silicon for Biomedical Applications*; Santos, H. A., Ed.; Woodhead Publishing, 2014; pp 185−222.
(24) Zucca, R. R. L.; Shen, Y. R. Wavelength-Modulation Spectra of Some Semiconductors. *Phys. Rev. B* **1970**, *1*, 2668−2676.
(25) Green, M. A. Self-Consistent Optical Parameters of Intrinsic Silicon at 300 K Including Temperature Coefficients. *Sol. Energy Mater. Sol. Cells* **2008**, *92*, 1305−1310.
(26) Albrecht, S.; Reining, L.; Del Sole, R.; Onida, G. *Ab Initio* Calculation of Excitonic Effects in the Optical Spectra of Semiconductors. *Phys. Rev. Lett.* **1998**, *80*, 4510−4513.
(27) Rohlfing, M.; Louie, S. G. Electron-Hole Excitations and Optical Spectra from First Principles. *Phys. Rev. B* **2000**, *62*, 4927−4944.
(28) Bayerl, D.; Kioupakis, E. Visible-Wavelength Polarized-Light Emission with Small-Diameter InN Nanowires. *Nano Lett.* **2014**, *14*, 3709−3714.
(29) ASTM G173-03: *Standard tables for reference solar spectral irradiances: direct normal and hemispherical on 37° tilted surface*. ASTM International: West Conshohoken, PA; 2003; doi: 10.1520/G0173-03R12.
(30) Ceperley, D. M.; Alder, B. J. Ground State of the Electron Gas by a Stochastic Method. *Phys. Rev. Lett.* **1980**, *45*, 566−569.
(31) Perdew, J. P.; Zunger, A. Self-Interaction Correction to Density-Functional Approximations for Many-Electron Systems. *Phys. Rev. B* **1981**, *23*, 5048.
(32) Ihm, J.; Zunger, A.; Cohen, M. L. Momentum-Space Formalism for the Total Energy of Solids. *J. Phys. C: Solid State Phys.* **1979**, *12*, 4409.
(33) Troullier, N.; Martins, J. L. Efficient Pseudopotentials for Plane-Wave Calculations. *Phys. Rev. B* **1991**, *43*, 1993−2006.
(34) Giannozzi, P.; Baroni, S.; Bonini, N.; Calandra, M.; Car, R.; Cavazzoni, C.; Ceresoli, D.; Chiarotti, G. L.; Cococcioni, M.; Dabo, I.; Corso, A. D.; de Gironcoli, S.; Fabris, S.; Fratesi, G.; Gebauer, R.; Gerstmann, U.; Gougoussis, C.; Kokalj, A.; Lazzeri, M.; Martin-Samos, L.; Marzari, N.; Mauri, F.; Mazzarello, R.; Paolini, S.; Pasquarello, A.; Paulatto, L.; Sbraccia, C.; Scandolo, S.; Sclauzero, G.; Seitsonen, A. P.; Smogunov, A.; Umari, P.; Wentzcovitch, R. M. QUANTUM ESPRESSO: A Modular and Open-Source Software Project for Quantum Simulations of Materials. *J. Phys.: Condens. Matter* **2009**, *21*, 395502.
(35) Hybertsen, M. S.; Louie, S. G. Electron Correlation in Semiconductors and Insulators: Band Gaps and Quasiparticle Energies. *Phys. Rev. B* **1986**, *34*, 5390−5413.
(36) Deslippe, J.; Samsonidze, G.; Strubbe, D. A.; Jain, M.; Cohen, M. L.; Louie, S. G. BerkeleyGW: A Massively Parallel Computer Package for the Calculation of the Quasiparticle and Optical Properties of Materials and Nanostructures. *Comput. Phys. Commun.* **2012**, *183*, 1269−1289.
(37) Deslippe, J.; Samsonidze, G.; Jain, M.; Cohen, M. L.; Louie, S. G. Coulomb-Hole Summations and Energies for *GW* Calculations with Limited Number of Empty Orbitals: A Modified Static Remainder Approach. *Phys. Rev. B* **2013**, *87*, 165124.
(38) Monkhorst, H. J.; Pack, J. D. Special Points for Brillouin-Zone Integrations. *Phys. Rev. B* **1976**, *13*, 5188−5192.

DOI: 10.1021/ph5002999
ACS Photonics 2015, 2, 208−215